Hindawi
Complexity
Volume 2021, Article ID 4113022, 15 pages
https://doi.org/10.1155/2021/4113022

Research Article

Collaborative Control of Multimotor Systems for Fixed-Time Optimisation Based on Virtual Main-Axis Speed Compensation Structure

Changfan Zhang,[1] **Mingjie Xiao**,[1] **Jing He**,[1] **Zhitian Liu**,[2] **Xingxing Yang**,[1] **Qian Zhang**,[1] **and Hongrun Chen**[1]

[1]*College of Electrical and Information Engineering, Hunan University of Technology, Zhuzhou 412000, China*
[2]*State Grid Fuyang City Chengjiao Electric Power Supply Company, Fuyang 236000, China*

Correspondence should be addressed to Jing He; hejing@263.net

Received 29 May 2021; Accepted 14 July 2021; Published 28 July 2021

Academic Editor: Xiao Ling Wang

In response to the high-speed and high-precision collaborative control requirements of the multimotor system for filling, a new type of virtual master-axis control structure is proposed and a multimotor fixed-time optimized collaborative control algorithm is designed. Firstly, coupling relationship between virtual and slave motors is effectively established by designing a velocity compensation module for the virtual motor. Secondly, the sliding mode observer (SMO) is used to reconstruct the composite disturbance composed of motor parameter perturbation and load disturbance. Finally, the variable gain terminal sliding mode controller (SMC) is designed to ensure that each slave motor can track the given value within a fixed time. The fast convergence of the system can be proved by the fixed-time convergence theorem and Lyapunov's stability theorem. The simulation results show that, compared with the traditional virtual main-axis control strategy, the proposed method is more effective for the tracking control of each slave motor in the initial stage.

1. Introduction

High-performance collaborative control of filling multimachine is one of the key technologies in the research and development of thick sauce and viscous food packaging equipment. It is also an important embodiment of high-speed and high-precision filling operation. At present, studies on filling multimachine collaborative control technologies usually focus on synchronous control of multimotor systems [1, 2]. In the multimotor synchronous control, the synchronous topology and control algorithm are two aspects worthy of attention. Therefore, the following is a summary of domestic and foreign research status from these two aspects.

Main multimotor synchronous control strategies for different synchronous topology structures are master-slave synchronous control [3], adjacent coupling synchronous control [4], relative coupling synchronous control [5], and virtual main-axis synchronous controls [6]. Yao et al. redefined adjacent cross-coupling error and designed auto disturbance rejection controller by extracting the Laplacian matrix [7]. Xu et al. proposed an optimal control strategy based on combined cross-coupling errors against various coupling errors and disturbance in multilayer and multiaxis control systems [8]. Huang et al. combined adjacent cross-coupling control strategy with adaptive algorithm to ease jitters when the speed is stable by considering phase and speed synchronisation control of multiactuators in the oscillation system [9]. Sun et al. combined fuzzy control technology with ring coupling synchronous structure to achieve the reliable operation of multimotor driving system [10]. Tao et al. proposed an improved adjacent coupling synchronous control strategy to simplify the structure of velocity synchronous control by introducing a new coupling

coefficient in the traditional adjacent coupling method [11]. Shi et al. put forward an improved multimotor relative coupling synchronous control, which also decoupled tracking and synchronisation errors of the system [12]. Zhang et al. mainly improved the relative coupling synchronization structure and then realized the smooth operation of the intelligent filling equipment for sticky food under complex working conditions [13]. Xu et al. investigated the adaptive synchronisation of coupled harmonic oscillator with switching topology and proposed an edge-based servo synchronous adaptive control protocol [14]. These control strategies promote the development of multimotor synchronous control technologies. However, the virtual main-axis control structure exerts a strong control effect on the application of multimotor synchronous technology with a unique feedback mechanism and characteristics of virtual motor as the navigator. Zhang and He explored a multimotor virtual main-axis control strategy based on the observer to reflect the dynamic relationship between virtual and slave motors accurately [15]. Lin and Cai estimated the composite disturbance of the motor using sliding mode observer to ensure that slave motors reach high synchronisation accuracy [16]. He and Chen focused on the total consensus control in multimotor cooperation to ensure that the total power of the system remains constant under power loss of a single motor [17].

The synchronous control algorithm mainly includes multiagent consensus [18, 19] and sliding mode variable structure control [20, 21] algorithms due to different design ideas of multimotor synchronous control. Xu and Li evaluated the multiagent consensus algorithm and proposed a semiglobal consensus control protocol based on low-gain state feedback with consideration for the intermittent semiglobal consensus problem of high-order multiagent system under input saturation [22]. Wang et al. analysed the structure of distributed observer of continuous linear time-invariant system and reduced the dependence of the system on topology structure information using adaptive rule [23]. Wang and Su investigated the collaborative control of linear time-invariant network system with uncertainty and constrained states of all agents by constructing an interval observer [24]. Liu and Su explored containment control of multiagent system based on data information of intermittent sampling position and obtained necessary and sufficient conditions for containment in the case of time delay and delay free [25]. Liu and Su further examined necessary and sufficient conditions, including control protocol under the condition of time delay, and effectively solved the problem of using the second-order multiagent system to control with only sampling position data [26]. Zheng et al. proposed an optimal operation model for microgrid based on the multiagent system to save the entire energy cost of locally observable convex function [27]. Fan and Wang assessed problems on following the consensus of a second-order multiagent system with input saturation and proved the stable consistency of the multiagent system using adaptive control technology [28]. Zhai et al. proposed a new pulse delay control method based on sampled data to realise the pulse synchronisation of multiagent systems [29]. Liu et al. examined the group controllability of the multiagent system, proposed a general definition of group controllability, and established a correlation criterion of group controllability [30]. In the research of sliding mode variable structure control algorithm, Shen et al. developed a trajectory tracking control scheme for the Mars orbiter and proposed a method of adaptive fixed-time control [31]. Shao et al. proposed a state observer with two polynomial feedback terms to identify unmeasurable speed states and unknown uncertain disturbances. The designed speedless fixed-time controller integrates the obtained observations [32]. Sun and Wang designed a sliding mode controller for angle tracking control of wearable exoskeleton based on model-free fixed-time control algorithm [33].

Although the multimachine cooperative control technology has been extensively investigated [34, 35], studies on multimachine high-performance collaborative control for thick sauce and viscous food filling are limited. In particular, the viscous characteristics of the filling material greatly hinder the speed and efficiency of the filling, resulting in two technical problems in the high-speed and high-precision operation of the filling multimotor system. (1) Virtual main-axis synchronous control is a common control strategy for filling multimotor production that can effectively improve the synchronisation accuracy of multimachine collaborative operation. The rotation speed of the slave filling conveying motor cannot be fed back to the virtual motor and the insufficient coupling correlation between them are limitations of the current feedback mechanism of the virtual main-axis control structure in terms of the multimotor collaborative control strategy. (2) As one of the effective controllers of the servo system, the sliding mode controller is widely used in various filling production occasions. Approaching speed of the existing sliding mode controller must be improved because its convergence speed demonstrates difficulty in meeting the requirements of high-speed operation of the servo system, especially when the sliding mode operation reaches the sliding surface from any initial position, in terms of the multimachine collaborative control algorithm.

Hence, a new multimotor collaborative control method for fixed-time optimisation based on the virtual main-axis structure is proposed in this study to solve these problems and meet the demand of the filling multimotor system for high-performance collaborative control. This study provides the following contributions:

(1) A speed compensator is added to the virtual motor to improve the existing virtual main-axis control structure, and the coupling relationship between virtual and slave motors in the speed is established given that the information on the velocity of slave motors and rotor position cannot be fed back to the virtual motor in the traditional virtual main-axis structure.

(2) A new type of variable gain terminal SMC is designed to realize the high-speed and high-precision synchronous control of the filling multimotor system. It mainly solves the problem of slow convergence speed when the system error reaches the terminal sliding surface from the initial state.

This paper is organized as follows: by taking advantage of the existing virtual main shaft synchronization control structure, a speed compensator is added to the virtual motor and the synchronization topology is improved in Section 2. The multimotor system model is established in Section 3. The sliding mode observer is used to overcome the parameter perturbation and load changes of the multimotor system in Section 4. The system controller is designed to ensure that the speed of each slave motor can quickly track the given value in Section 5. The experimental simulation is presented in Section 6. Finally, the conclusion is given in Section 7.

2. Improved Virtual Main Shaft Control Structure Design

A virtual main-axis control structure with speed compensator is designed for the multimotor synchronous technology in this section on the basis of fully absorbing the characteristics and principles of the existing virtual main-axis strategy. Specific details of each module of this control structure designed are shown in Figure 1.

Figure 1 shows the permanent magnet synchronous motor (PMSM) model, virtual motor, tracking error of permanent magnet synchronous motor, sliding mode function, controller module, virtual controller module, observer module, and virtual motor speed compensator as well as detailed formulas, logical relations, and related variables of each module. Compared with the diagrams of various modules shown in Figure 1, the golden area is the proposed virtual motor speed compensator designed in this study. The compensation signal generated by the virtual motor compensator can be directly fed back to the virtual motor and can also be adjusted by selecting a suitable virtual motor's moment of inertia. Although the compensation signal is known and available, $\omega_{\text{vir}} - \omega_j$ are bounded variables. Therefore, the output value of the virtual motor speed compensator is regarded as a variable with a known upper bound that can reduce the design difficulty and calculation of the virtual motor controller. The blue area denotes the designed variable-gain terminal SMC in this study. A dynamic switching gain term, including the sliding mode function, is designed to improve the convergence speed of the sliding mode movement because the tracking error of each slave motors is large in the initial state.

3. Establishment of the Multimotor System Model

The PMSM of the driving system for filling production is the research object of this study. The second-order kinetic model of motor j in the multimotor system can be expressed as follows [13]:

$$\begin{cases} \dot{\theta}_j = \omega_j, \\ \dot{\omega}_j = -a_j\omega_j + b_j u_j - p_j T_{Lj}, \end{cases} \quad j = 1, 2, \ldots, n, \tag{1}$$

where $a_j = R_{\Omega j}/J_j$; $b_j = 3/2 \cdot n_{pj}^2 \psi_{fj}/J_j$; $p_j = n_{pj}/J_j$; $u_j = i_{qj}$; θ_j and $w_j$are the position and electrical angular velocity of the motor rotor, respectively; T_{Lj} is the load torque on the shaft; $R_{\Omega j}$ is the rotational resistance coefficient; n_{Pj} is the number of pole pairs; J_j is the moment of inertia; Ψ_{fj} is the rotor flux; i_{qj} is the q-axis components of the stator current; and u_j is the controller to be designed.

The state equation of virtual motor based on formula (1) is expressed as follows:

$$\begin{cases} \dot{\theta}_{\text{vir}} = \omega_{\text{vir}}, \\ \dot{\omega}_{\text{vir}} = -a_{\text{vir}}\omega_{\text{vir}} + b_{\text{vir}}u_{\text{vir}} - p_{\text{vir}}T_{\text{Lvir}}, \end{cases} \tag{2}$$

where $a_{\text{vir}} = R_{\Omega\text{vir}}/J_{\text{vir}}$; $b_{\text{vir}} = 3/2 \cdot n_{p\text{vir}}^2 \psi_{f\text{vir}}/J_{\text{vir}}$; $p_{\text{vir}} = n_{p\text{vir}}/J_{\text{vir}}$; $u_{\text{vir}} = i_{q\text{vir}}$; θ_{vir} and ω_{vir} are the virtual motor rotor position and electrical angular velocity, respectively; $T_{L\text{vir}}$ is the virtual motor load torque; $R_{\Omega\text{vir}}$ is the virtual motor rotational resistance coefficient of motor; $n_{p\text{vir}}$ is the number of pole pairs of virtual motor; J_{vir} is the virtual motor moment of inertia; $\psi_{f\text{vir}}$ is the virtual motor rotor flux; $i_{q\text{vir}}$ is the virtual motor q-axis components of the stator current; and $u_{\text{vir}}$is the virtual controller to be designed.

Motor parameters will be subjected to uncertain perturbation during long-time operation of the motor, and the motor load torque will change uncertainly due to the change of filling materials in the filling process. Hence, formula (1) can be transformed into the following:

$$\begin{cases} \dot{\theta}_j = \omega_j, \\ \dot{\omega}_j = -\left(\overline{a}_j + \Delta a_j\right)\omega_j + \left(\overline{b}_j + \Delta b_j\right)u_j - p_j\Delta T_{Lj}, \end{cases} \quad j = 1, 2, \ldots, n, \tag{3}$$

where $\overline{a}_j, \overline{b}_j$ refer to nominal values of system parameters, $\Delta a_j, \Delta b_j$ refer to perturbation values of system parameters, and ΔT_{Lj} refers to the variation of load torque of the filling motor. These variables are considered unknown composite disturbances d_j. Hence, formula (3) can be modified as follows:

$$\begin{cases} \dot{\theta}_j = \omega_j, \\ \dot{\omega}_j = -\overline{a}_j\omega_j + \overline{b}_j u_j + d_j, \end{cases} \quad j = 1, 2, \ldots, n, \tag{4}$$

where $d_j = -\Delta a_j\omega_j + \Delta b_j u_j - p_j\Delta T_{Lj}$.

Define the vector form of each state variable as $\boldsymbol{\theta} = [\theta_1, \ldots, \theta_j, \ldots, \theta_n]^T$; $\boldsymbol{\omega} = [\omega_1, \ldots, \omega_j, \ldots, \omega_n]^T$; $\mathbf{u} = [u_1, \ldots, u_j, \ldots, u_n]^T$; and $\mathbf{d} = [d_1, \ldots, d_j, \ldots, d_n]^T$.

Formula (4) is modified in the following matrix form:

$$\begin{cases} \dot{\boldsymbol{\theta}} = \boldsymbol{\omega}, \\ \dot{\boldsymbol{\omega}} = -\mathbf{a}\boldsymbol{\omega} + \mathbf{b}\mathbf{u} + \mathbf{d}, \end{cases} \tag{5}$$

where $\mathbf{a} = \text{diag}\{\overline{a}_1, \ldots, \overline{a}_j, \ldots, \overline{a}_n\}$ and $\mathbf{b} = \text{diag}\{\overline{b}_1, \ldots, \overline{b}_j, \ldots, \overline{b}_n\}$ are coefficient matrices.

4. Sliding Mode Observer Design and Stability Analysis

The composite disturbance d_j of the motor system included in formula (4) will exert a strong influence on the synchronous performance. Therefore, the SMO will be introduced in this section to explore d_j.

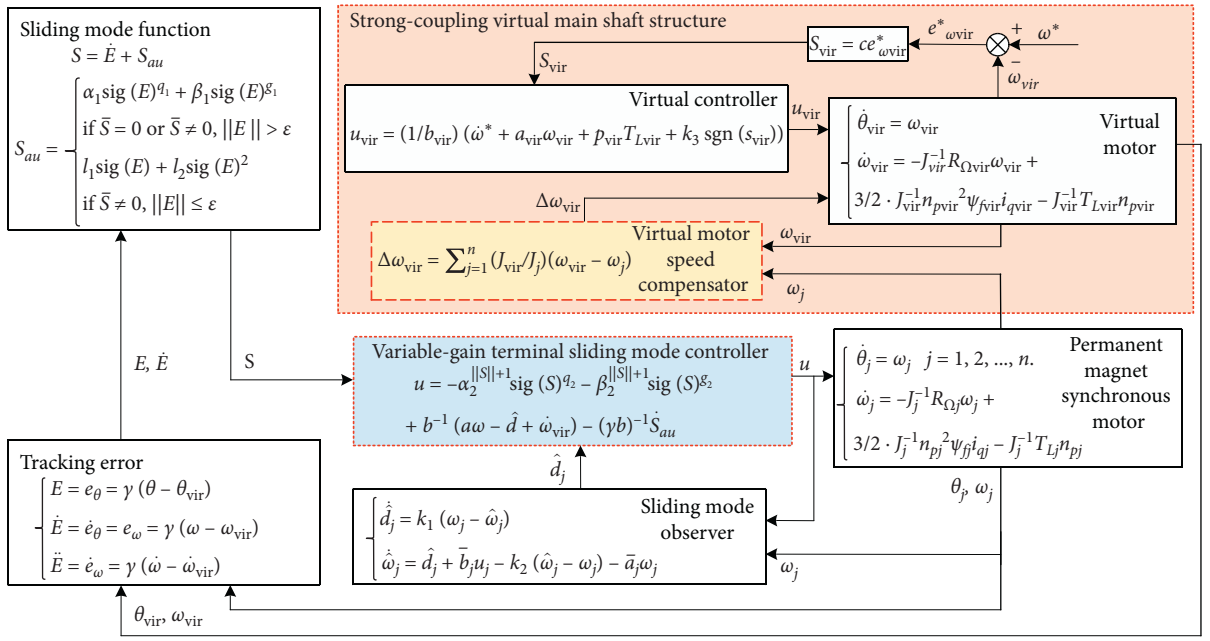

FIGURE 1: The schematic diagram of specific details of each module of this control structure.

The observer is designed for system (4) as follows [36]:

$$\begin{cases} \dot{\hat{\theta}}_j = \hat{\omega}_j + k_1 \mathrm{sgn}\left(\theta_j - \hat{\theta}_j\right), \\ \dot{\hat{\omega}}_j = -\bar{a}_j\omega_j + \bar{b}_j u_j + k_2 \mathrm{sgn}\left(\omega_j - \hat{\omega}_j\right), \\ \qquad\qquad j = 1, 2, \ldots, n, \end{cases} \tag{6}$$

where $\hat{\theta}_j$ and $\hat{\omega}_j$ refer to observed values of rotor position and speed of motor j, respectively, and k_1, k_2 refer to the parameters to be designed.

The observational error vector is defined as $\tilde{\mathbf{e}}_j = [\tilde{\theta}_j\ \tilde{\omega}_j]^T = [\theta_j - \hat{\theta}_j\ \omega_j - \hat{\omega}_j]^T$, and $\tilde{\theta}_j, \tilde{\omega}_j$ refer to observational errors of the rotor position and speed of motor j, respectively.

Hypothesis 1. A normal number $|d_j|_{\max}$ and $d_j \leq |d_j|_{\max}$ exist given that perturbation values of motor parameters $\Delta a_j, \Delta b_j$ and load torque variation ΔT_{Lj} are bounded in practice.

Theorem 1. *Observer (6) corresponding to motor j is designed for filling multimotor system (4). If $k_1 > |\tilde{\omega}_j|_{\max} + \eta_1, k_2 > |d_j|_{\max} + \eta_2$, $(j = 1, 2, \ldots, n)$ is satisfied, then the observational error can converge to 0 in a limited time $T_{\tilde{e}_j}$. The composite disturbance d_j can be expressed as follows:*

$$\lim_{x \longrightarrow T_{\tilde{e}_j}} \hat{d}_j = d_j = k_2 \mathrm{sgn}\left(k_1 \mathrm{sgn}\left(\theta_j - \hat{\theta}_j\right)\right). \tag{7}$$

Proof. The error equation of the observer system can be obtained when formula (6) is subtracted from formula (4) as follows:

$$\begin{cases} \dot{\tilde{\theta}}_j = \tilde{\omega}_j - k_1 \mathrm{sgn}\left(\tilde{\theta}_j\right), \\ \dot{\tilde{\omega}}_j = d_j - k_2 \mathrm{sgn}\left(\tilde{\omega}_j\right). \end{cases} \tag{8}$$

The selected sliding mode surface of the SMO is expressed as follows:

$$\mathbf{s}_{\tilde{e}_j} = \tilde{e}_j. \tag{9}$$

Take the derivative of the above formula and substitute formula (8) into it to get

$$\dot{s}_{\tilde{e}_j} = \dot{\tilde{e}}_j = \begin{bmatrix} \dot{\tilde{\theta}}_j & \dot{\tilde{\omega}}_j \end{bmatrix}^T = \left[\tilde{\omega}_j - k_1 \mathrm{sgn}\left(\tilde{\theta}_j\right)\ \ d_j - k_2 \mathrm{sgn}\left(\tilde{\omega}_j\right)\right]^T. \tag{10}$$

The Lyapunov function of the observer is expressed as follows:

$$V_{\tilde{\mathbf{e}}_j} = \frac{1}{2}\tilde{e}_j^T\tilde{e}_j. \tag{11}$$

The following equation can be derived from formula (11):

$$\begin{aligned} \dot{V}_{\tilde{e}_j} &= \tilde{e}_j^T\dot{\tilde{e}}_j = \tilde{\theta}_j\left[\tilde{\omega}_j - k_1 \mathrm{sgn}\left(\tilde{\theta}_j\right)\right] + \tilde{\omega}_j\left[d_j - k_2 \mathrm{sgn}\left(\tilde{\omega}_j\right)\right] \\ &= \tilde{\theta}_j\tilde{\omega}_j - k_1\left|\tilde{\theta}_j\right| + \tilde{\omega}_j d_j - k_2\left|\tilde{\omega}_j\right| \\ &\leq \left|\tilde{\theta}_j\right|\left(\left|\tilde{\omega}_j\right| - k_1\right) + \left|\tilde{\omega}_j\right|\left(\left|d_j\right| - k_2\right) \\ &\leq -\min\left\{k_1 - \left|\tilde{\omega}_j\right|, k_2 - \left|d_j\right|\right\}\left\|\tilde{e}_j\right\|. \end{aligned} \tag{12}$$

If the designed parameters meet $k_1 > |\tilde{\omega}_j|_{\max} + \eta_1, k_2 > |d_j|_{\max} + \eta_2$ and $\eta_1, \eta_2 > 0$, then the following equation can be obtained:

$$\dot{V}_{\tilde{e}_j} \leq -min\{\eta_1, \eta_2\}\left\|\tilde{e}_j\right\| = -\eta\left\|\tilde{e}_j\right\|, \tag{13}$$

where $\eta = \min\{\eta_1, \eta_2\}$.

Therefore, if $\tilde{\theta}_j \longrightarrow 0, \tilde{\omega}_j \longrightarrow 0$, then $\dot{V}_{\tilde{e}_j} \leq 0$ and $V_{\tilde{e}_j} \longrightarrow 0$. The observer system (6) at this moment demonstrates asymptotic stability. According to Hypothesis 1, the time when the observer system reaches the sliding surface is a limited value $T_{\tilde{e}_j}$. The following conclusions can be obtained from formulas (9) and (10) and the principle [37] of sliding mode equivalence when $t > T_{\tilde{e}_j}$:

$$\begin{cases} s_{\tilde{e}_j} = 0 \\ \dot{s}_{\tilde{e}_j} = 0 \end{cases} \Rightarrow \begin{cases} \theta_j = \hat{\theta}_j, \\ \tilde{\omega}_j = k_1 \mathrm{sgn}\left(\tilde{\theta}_j\right) = k_1 \mathrm{sgn}\left(\theta_j - \hat{\theta}_j\right), \end{cases} \begin{cases} \omega_j = \hat{\omega}_j, \\ d_j = k_2 \mathrm{sgn}\left(\tilde{\omega}_j\right) = k_2 \mathrm{sgn}\left(\omega_j - \hat{\omega}_j\right). \end{cases} \tag{14}$$

The unknown composite disturbance d_j can then be restructured as follows:

$$\lim_{x \longrightarrow T_{\tilde{e}_j}} \hat{d}_j = d_j = k_2 \mathrm{sgn}\left(k_1 \mathrm{sgn}\left(\theta_j - \hat{\theta}_j\right)\right). \tag{15}$$

If $t > t_1$ when $\forall \delta > 0, \exists t_1 < T_{\tilde{e}_j}$, then

$$\left|\hat{d}_j - d_j\right| < \delta. \tag{16}$$

Hence, the stability of the SMO has been proven. □

5. System Controller Design and Stability Analysis

Definition 1 (see [38]). $\mathrm{diag}(\mathbf{x})$ refers to the diagonal matrix of Vector $\mathbf{x}$ for any vector $\mathbf{x} = [x_1, x_2, \ldots, x_n]^T \in \mathbf{R}^n$ and expressed as follows:

$$\begin{cases} \mathbf{x}^a = \left[x_1^a, x_2^a, \ldots, x_n^a\right]^T, \\ |\mathbf{x}|^p = \left[|x_1|^a, |x_2|^a, \ldots, |x_n|^a\right]^T, \\ \mathrm{sgn}(\mathbf{x}) = \left[\mathrm{sgn}(x_1), \mathrm{sgn}(x_2), \ldots, \mathrm{sgn}(x_n)\right]^T, \\ \mathrm{sig}(\mathbf{x})^a = \left[\mathrm{sgn}(x_1)|x_1|^a, \mathrm{sgn}(x_2)|x_2|^a, \ldots, \mathrm{sgn}(x_n)|x_n|^a\right]^T, \end{cases} \tag{17}$$

where $\mathrm{sgn}(\cdot)$ represents the standard symbolic function and a refers to an arbitrary real number.

Lemma 1 (see [39]). *Stability theorem of fixed-time) For the system is expressed as follows:*

$$\dot{x}(t) = f(x(t)), f(0) = 0, t_0 = 0, x_0 \triangleq x(0), \tag{18}$$

where $x(t) \in R^n$ represents the state of the system, $f: U \longrightarrow R^n$ refers to a continuous function from the domain containing the original point U to n_dimensional space R^n, $0 \in \mathbf{R}^n$ represents the zero vector, and x_0 is defined as the initial state.

If a positive definite and continuous function $V(x)$ exists in the domain U, then

$$\dot{V}(x) \leq -\alpha V(x)^p - \beta V(x)^g, \quad x \in U \backslash \{0\}, \tag{19}$$

where α, β, γ, p, and g are normal numbers that meet $p < 1$ and $g > 1$, respectively, and the system is stable in the fixed time. Hence, the system state can converge to the equilibrium point in a fixed time independent of the initial value.

$$T \leq \frac{1}{\alpha(1-p)} + \frac{1}{\beta(g-1)}. \tag{20}$$

5.1. Design and Stability Analysis of the Virtual Sliding Mode Controller. The virtual controller u_{vir} can be used to control the velocity of the virtual motor in this study given that the upper bound of the virtual motor speed compensator signal is known. The tracking error $e^*_{\omega \mathrm{vir}}$ of the speed of the virtual motor is expressed as follows:

$$e^*_{\omega \mathrm{vir}} = \omega^* - \omega_{\mathrm{vir}}. \tag{21}$$

The following design of the virtual motor speed compensator module is added:

$$\Delta\omega_{\mathrm{vir}} = \sum_{j=1}^{n} \frac{J_{\mathrm{vir}}}{J_j}\left(\omega_{\mathrm{vir}} - \omega_j\right). \tag{22}$$

This signal can reduce the compensation by appropriately increasing the inertia J_j of the virtual motor to improve the convenience in parameter selection of the virtual controller. Meanwhile, $\Delta\omega_{\mathrm{vir}}$ is also a bounded variable, that is, $\Delta\omega_{\mathrm{vir}} \leq |\Delta\omega_{\mathrm{vir}}|_{\max}$, because ω_{vir} and ω_j are both bounded variables.

The second-order system model of the improved virtual main-axis structure can be obtained from formulas (2) and (22) as follows:

$$\begin{cases} \dot{\theta}_{\mathrm{vir}} = \omega_{\mathrm{vir}}, \\ \dot{\omega}_{\mathrm{vir}} = -a_{\mathrm{vir}}\omega_{\mathrm{vir}} + b_{\mathrm{vir}}u_{\mathrm{vir}} - p_{\mathrm{vir}}T_{L\mathrm{vir}} - \Delta\omega_{\mathrm{vir}}. \end{cases} \tag{23}$$

The following sliding mode surface of the virtual controller is selected:

$$s_{\mathrm{vir}} = ce^*_{\omega \mathrm{vir}}, \tag{24}$$

where c refers to the normal number to be designed.

The virtual controller is designed as follows:

$$u_{\mathrm{vir}} = \frac{1}{b_{\mathrm{vir}}}\left(\dot{\omega}^* + a_{\mathrm{vir}}\omega_{\mathrm{vir}} + p_{\mathrm{vir}}T_{L\mathrm{vir}} + k_3 \mathrm{sgn}\left(s_{\mathrm{vir}}\right)\right). \tag{25}$$

Theorem 2. *Virtual controller (2) is shown in formula (25). If the coefficient of the control can meet $k_3 > |\Delta\omega_{vir}|_{\max} + \eta_3$, then $e^*_{\omega vir}$ will gradually converge to 0.*

Proof. Define the Lyapunov function of the virtual controller as

$$V_{\text{vir}} = \frac{1}{2}s^2_{\text{vir}}. \tag{26}$$

The following equation can be derived from formula (26):

$$\dot{V}_{\text{vir}} = s_{\text{vir}}\dot{s}_{\text{vir}} = s_{\text{vir}}c\dot{e}^*_{\text{vir}} = s_{\text{vir}}c\left(\dot{\omega}^* + a_{\text{vir}}\omega_{\text{vir}} - b_{\text{vir}}u_{\text{vir}} + p_{\text{vir}}T_{L\text{vir}} + \Delta\omega_{\text{vir}}\right). \tag{27}$$

The following equation can be obtained by substituting formula (25) into formula (27):

$$\dot{V}_{\text{vir}} = s_{\text{vir}}c\left(-k_3\text{sgn}\left(s_{\text{vir}}\right) + \Delta\omega_{\text{vir}}\right) = -c\left(k_3\left|s_{\text{vir}}\right| - s_{\text{vir}}\Delta\omega_{\text{vir}}\right). \tag{28}$$

The following can be obtained when η_3 is any small normal number that only guarantees $k_3 > |\Delta\omega_{\text{vir}}|_{\max} + \eta_3$:

$$\dot{V}_{\text{vir}} < 0. \tag{29}$$

Formula (29) and the equivalent principle of sliding mode [37] showed that $e^*_{\omega\text{vir}}$ converges to 0 when $\omega^* = \omega_{\text{vir}}$.

Hence, the stability of the virtual motor controller has been proven. □

5.2. Design and Stability Analysis of the Filling Motor Controller. The tracking error of each slave motor is defined as follows:

$$\mathbf{e_\theta} = \boldsymbol{\gamma}\left(\boldsymbol{\theta} - \boldsymbol{\theta}_{\mathbf{vir}}\right) = \left[e_{\theta_1}, \ldots, e_{\theta_j}, \ldots, e_{\theta_n}\right]^T_{1\times n} = \left[\gamma_{1,\text{vir}}\left(\theta_1 - \theta_{\text{vir}}\right), \ldots, \gamma_{\text{j,vir}}\left(\theta_j - \theta_{\text{vir}}\right), \ldots, \gamma_{\text{n,vir}}\left(\theta_n - \theta_{\text{vir}}\right)\right]^T_{1\times n}, \tag{30}$$

$$\mathbf{e_\omega} = \dot{\mathbf{e}}_{\boldsymbol{\theta}} = \boldsymbol{\gamma}\left(\omega - \omega_{\mathbf{vir}}\right) = \left[e_{\omega_1}, \ldots, e_{\omega_j}, \ldots, e_{\omega_n}\right]^T_{1\times n} = \left[\gamma_{1,\text{vir}}\left(\omega_1 - \omega_{\text{vir}}\right), \ldots, \gamma_{j,\text{vir}}\left(\omega_j - \omega_{\text{vir}}\right), \ldots, \gamma_{n,\text{vir}}\left(\omega_n - \omega_{\text{vir}}\right)\right]^T_{1\times n}, \tag{31}$$

where $\gamma_{1,\text{vir}} = J_1/J_{\text{vir}}, \ldots, \gamma_{j,\text{vir}} = J_j/J_{\text{vir}}, \ldots, \gamma_{n,\text{vir}} = J_n/J_{\text{vir}}$; $\boldsymbol{\gamma} = \text{diag}\left\{\gamma_{1,\text{vir}}, \cdots, \gamma_{j,\text{vir}}, \cdots, \gamma_{n,\text{vir}}\right\}$; $\boldsymbol{\theta}_{\mathbf{vir}} = [\theta_{\text{vir}}, \ldots, \theta_{\text{vir}}, \ldots, \theta_{\text{vir}}]^T_{1\times n}$; and $\boldsymbol{\omega}_{\mathbf{vir}} = [\omega_{\text{vir}}, \ldots, \omega_{\text{vir}}, \ldots, \omega_{\text{vir}}]^T_{1\times n}$.

The simplification of this error equation obtained from formulas (30) and (31) can be expressed as follows:

$$\begin{cases} \mathbf{E} = \mathbf{e_\theta} = \boldsymbol{\gamma}\left(\boldsymbol{\theta} - \boldsymbol{\theta}_{\mathbf{vir}}\right), \\ \dot{\mathbf{E}} = \dot{\mathbf{e}}_{\boldsymbol{\theta}} = \mathbf{e}_\omega = \boldsymbol{\gamma}\left(\boldsymbol{\omega} - \boldsymbol{\omega}_{\mathbf{vir}}\right), \\ \ddot{\mathbf{E}} = \dot{\mathbf{e}}_\omega = \boldsymbol{\gamma}\left(\dot{\boldsymbol{\omega}} - \dot{\boldsymbol{\omega}}_{\mathbf{vir}}\right). \end{cases} \tag{32}$$

The selected terminal sliding surface is expressed as follows [38, 40]:

$$\mathbf{S} = \dot{E} + \mathbf{S}_{\text{au}}, \tag{33}$$

where

$$\mathbf{S_{au}} = \begin{cases} \alpha_1\text{sig}\left(\mathbf{E}\right)^{q_1} + \beta_1\text{sig}\left(\mathbf{E}\right)^{g_1}, & \text{if } \overline{\mathbf{S}} = \mathbf{0} \text{ or } \overline{\mathbf{S}} \neq \mathbf{0}, \|\mathbf{E}\| > \varepsilon, \\ l_1\text{sig}\left(\mathbf{E}\right) + l_2\text{sig}\left(\mathbf{E}\right)^2, & \text{if } \overline{\mathbf{S}} \neq \mathbf{0}, \|\mathbf{E}\| \leq \varepsilon, \end{cases} \tag{34}$$

where $\overline{\mathbf{S}} = \dot{\mathbf{E}} + \alpha_1\text{sig}\left(\mathbf{E}\right)^{q_1} + \beta_1\text{sig}\left(\mathbf{E}\right)^{g_1}$. α_1, β_1 refer to the coefficients to be designed that meet $\alpha_1 > 1, \beta_1 > 1$. q_1 and g_1 satisfy $q_1 \in (0.5, 1)$ and $g_1 > 1$, respectively. ε refers to the switching threshold. $\mathbf{S_{au}}$ and $\dot{S}_{\mathbf{au}}$ are continuous functions in $\|\mathbf{E}\| = \varepsilon$. $l_1 = 0.5\alpha_1\varepsilon^{q_1-1} + 0.5\beta_1\varepsilon^{g_1-1}$; $l_2 = 0.5\alpha_1\varepsilon^{q_1-2} + 0.5\beta_1\varepsilon^{g_1-2}$.

This switching rule (34) is inspired by [41, 42] to avoid the singularity.

The optimized variable gain terminal SMC is designed as follows:

$$\mathbf{u} = -\alpha_2^{\|\mathbf{S}\|+1}\text{sig}\left(\mathbf{S}\right)^{q_2} - \beta_2^{\|\mathbf{S}\|+1}\text{sig}\left(\mathbf{S}\right)^{g_2} + \mathbf{b}^{-1}\left(\mathbf{a}\boldsymbol{\omega} - \widehat{\mathbf{d}} + \dot{\boldsymbol{\omega}}_{\text{vir}}\right) - \left(\boldsymbol{\gamma}\mathbf{b}\right)^{-1}\dot{\mathbf{S}}_{\mathbf{au}}, \tag{35}$$

where α_2, β_2 refer to coefficients to be designed that meet $\alpha_2 > 1, \beta_2 > 1$, respectively, and q_2 and g_2 satisfy $q_2 \in (0.5, 1)$ and $g_2 > 1$, respectively.

Theorem 3. *The system controller is designed in formula (35). If the coefficient of the controller satisfies $\alpha_2 > 1, \beta_2 > 1$, $q_2 \in (0.5, 1)$, and $g_2 > 1$, then the system error (32) in formula*

(5) will converge to 0 within the fixed-time $T_2 + T_3$. The upper bound on this time of convergence is

$$\begin{cases} T_2 \le \dfrac{1}{\alpha_2^{\|S\|+1}\lambda_{\min}[(\mathbf{I}+\boldsymbol{\gamma})\mathbf{b}]\left(1-\theta_{q1}\right)(1-q_2)} + \dfrac{1}{2^{1-g_2}\beta_2^{\|S\|+1}\lambda_{\min}[(\mathbf{I}+\boldsymbol{\gamma})\mathbf{b}]\left(1-\theta_{g1}\right)(g_2-1)}, \\ T_3 \le \dfrac{1}{\alpha_1\left(1-\theta_{q_2}\right)(1-q_1)} + \dfrac{1}{2^{1-g_1}\beta_1\left(1-\theta_{g_2}\right)(g_1-1)}. \end{cases} \tag{36}$$

Proof. Define the Lyapunov function of the optimized variable gain terminal SMC as

$$V_{\mathbf{S}} = \mathbf{S}^{\mathbf{T}}\mathbf{S}. \tag{37}$$

Substituting formulas (32) and (33) into formula (37) gives the following:

$$\dot{V}_{\mathbf{S}} = 2\mathbf{S}^{\mathbf{T}}\dot{S} = 2\mathbf{S}^{\mathbf{T}}\left[\boldsymbol{\gamma}\left(\dot{\omega}-\dot{\omega}_{\mathbf{vir}}\right)+\dot{S}_{\mathrm{au}}\right]. \tag{38}$$

Substituting formulas (5) and (35) into formula (38) gives the following:

$$\begin{aligned} \dot{V}_S &= 2\mathbf{S}^T\left[-\alpha_2^{\|S\|+1}\gamma b\,\mathrm{sig}(\mathbf{S})^{q_2} - \beta_2^{\|S\|+1}\gamma b\,\mathrm{sig}(\mathbf{S})^{g_2}\right] \\ &\le -2\alpha_2^{\|S\|+1}\lambda_{\min}(\boldsymbol{\gamma}\mathbf{b})\left[\left(|s_1|^2\right)^{q_2+1/2} + \left(|s_2|^2\right)^{q_2+1/2} + \cdots + \left(|s_n|^2\right)^{q_2+1/2}\right] \\ &\quad -2\beta_2^{\|S\|+1}\lambda_{\min}(\boldsymbol{\gamma}\mathbf{b})\left[\left(|s_1|^2\right)^{g_2+1/2} + \left(|s_2|^2\right)^{g_2+1/2} + \cdots + \left(|s_n|^2\right)^{g_2+1/2}\right]. \end{aligned} \tag{39}$$

The following can be obtained on the basis of the conclusion in [43]:

$$\dot{V}_{\mathbf{S}} \le -2\alpha_2^{\|\mathbf{S}\|+1}\lambda_{\min}(\boldsymbol{\gamma}\mathbf{b})V_{\mathbf{S}}^{q_2+1/2} - 2^{2-g_2}\beta_2^{\|\mathbf{S}\|+1}\lambda_{\min}(\boldsymbol{\gamma}\mathbf{b})V_{\mathbf{S}}^{g_2+1/2}. \tag{40}$$

According to Lemma 1, formula (40) satisfies the fixed-time convergence condition, and its time upper bound is expressed as

$$T_2 \le \frac{1}{\alpha_2^{\|\mathbf{S}\|+1}\lambda_{\min}[(\mathbf{I}+\boldsymbol{\gamma})\mathbf{b}]\left(1-\theta_{q1}\right)(1-q_2)} + \frac{1}{2^{1-g_2}\beta_2^{\|\mathbf{S}\|+1}\lambda_{\min}[(\mathbf{I}+\boldsymbol{\gamma})\mathbf{b}]\left(1-\theta_{g1}\right)(g_2-1)}. \tag{41}$$

□

Remark 1. Formula (41) shows that nonlinear coefficients $\alpha_1^{\|\mathbf{S}\|+1}$ and $\beta_1^{\|\mathbf{S}\|+1}$ satisfy the conditions of fixed-time convergence in the convergence of $\mathbf{S}$.

Assuming that $\mathbf{S} = \varphi$ exists at the moment T_φ within T_2, formula (41) shows the following upper bound of the time when the sliding mode movement moves from an arbitrary initial position to the sliding surface:

$$T_{\boldsymbol{\varphi}} = \frac{1}{\alpha_2^{\|\boldsymbol{\varphi}\|+1}\lambda_{\min}[(\mathbf{I}+\boldsymbol{\gamma})\mathbf{b}]\left(1-\theta_{q1}\right)(1-q_2)} + \frac{1}{2^{1-g_2}\beta_2^{\|\boldsymbol{\varphi}\|+1}\lambda_{\min}[(\mathbf{I}+\boldsymbol{\gamma})\mathbf{b}]\left(1-\theta_{g1}\right)(g_2-1)}. \tag{42}$$

The comparison of formula (42) with the method proposed in [43] shows that

$$T_{\boldsymbol{\varphi}} < \frac{1}{\alpha_2 \lambda_{\min}[(\mathbf{I}+\boldsymbol{\gamma})\mathbf{b}]\left(1-\theta_{q1}\right)\left(1-q_2\right)} + \frac{1}{2^{1-g_2}\beta_2 \lambda_{\min}[(\mathbf{I}+\boldsymbol{\gamma})\mathbf{b}]\left(1-\theta_{g1}\right)\left(g_2-1\right)}. \tag{43}$$

Remark 2. The comprehensive analysis of formulas (41) and (42) showed that the large gain coefficient of the sig function in the controller accelerates the speed to the sliding surface when the sliding mode movement moves away from $\mathbf{S} = 0$. The gain coefficient of the sig function will continuously approach α_1 and β_1 when the SM movement is close to $\mathbf{S} = 0$. Therefore, the actual convergence time will be shortened. In the process of sliding mode movement from the initial state to the sliding surface, the optimized SMC has better convergence performance than the original terminal SMC.

The following can be obtained from the above conclusion and formula (33) when the sliding mode movement reaches the sliding surface:

$$\dot{E} = -\mathbf{S}_{\mathrm{au}}. \tag{44}$$

In the process that the system moves to the equilibrium point on the sliding surface, based on sliding mode substitution method designed in formula (34), the classification should be discussed here.

When $\|\mathbf{E}\| > \varepsilon$, we can get

$$\dot{E} = -\alpha_1 \mathrm{sig}(\mathbf{E})^{q_1} - \beta_1 \mathrm{sig}(\mathbf{E})^{g_1}. \tag{45}$$

The Lyapunov function is defined, and the system error is analysed as follows:

$$V_{\mathbf{E}} = \mathbf{E}^{\mathbf{T}}\mathbf{E}. \tag{46}$$

The following can be obtained on the basis of formula (46):

$$\dot{V}_{\mathbf{E}} = 2\mathbf{E}^{\mathbf{T}}\dot{E}. \tag{47}$$

The following can be obtained after substituting formula (45) into formula (47):

$$\dot{V}_{\mathbf{E}} = 2\mathbf{E}^{\mathbf{T}}\left[-\alpha_1 \mathrm{sig}(\mathbf{E})^{q_1} - \beta_1 \mathrm{sig}(\mathbf{E})^{g_1}\right] \leq -2\alpha_1 V_{\mathbf{E}}^{(q_1+1)/2} - 2^{2-g_1}\beta_1 V_{\mathbf{E}}^{(g_1+1)/2}. \tag{48}$$

According to Lemma 1, formula (48) satisfies the fixed-time convergence condition, and the upper bound of time is expressed as follows:

$$T_3 \leq \frac{1}{\alpha_1\left(1-\theta_{q_2}\right)\left(1-q_1\right)} + \frac{1}{2^{1-g_1}\beta_1\left(1-\theta_{g_2}\right)\left(g_1-1\right)}, \tag{49}$$

where θ_{q2} and θ_{g2} refer to arbitrary normal numbers in the interval $(0, 1)$.

Formulas (41) and (49) demonstrate that the system error $\mathbf{E}$ will converge to 0 when the sliding mode moves for $t > T_2 + T_3$.

When $\|\mathbf{E}\| > \varepsilon$, we can get

$$\dot{E} = -l_1 \mathrm{sig}(\mathbf{E}) - l_2 \mathrm{sig}(\mathbf{E})^2. \tag{50}$$

Similarly, the system error is also analysed as follows:

$$\dot{V}_{\mathbf{E}} = 2\mathbf{E}^{\mathbf{T}}\left[-l_1 \mathrm{sig}(\mathbf{E}) - l_2 \mathrm{sig}(\mathbf{E})^2\right] \leq -2l_1 V_{\mathbf{E}}. \tag{51}$$

Hence, formula (51) shows that $V_{\mathbf{E}}$ will converge to 0 exponentially given that l_1 is a positive real number.

Remark 3. The comprehensive analysis on formulas (45)–(51) shows that the convergence time of the linear sliding surface of $\mathbf{S_{au}} = l_1 \mathrm{sig}(\mathbf{E}) + l_2 \mathrm{sig}(\mathbf{E})^2$ instead of the terminal sliding mode can be ignored if the value of ε is sufficiently small. The convergence time is approximately equal to T_2 in this case. Therefore, system errors $\|\mathbf{E}\|$ and $\|\dot{E}\|$ can converge to 0 within $T_2 + T_3$; that is, the velocity of all motors in the multimotor system can achieve $\omega = \omega_{\mathbf{vir}}$ in a fixed time. Moreover, filling motors can track the given value in real time because the velocity of the virtual motor is $\omega_{\mathrm{vir}} = \omega^*$. Hence, the stability of the filling motor controller has been proven.

The overall control block of the improved virtual main-axis system is shown in Figure 2 to understand the content of Figure 1 and design details of each module further.

Figure 2 shows that the most important characteristic of the control structure is the addition of the speed compensator to the virtual motor and the use of the virtual controller to provide feedback and adjust the tracking error and compensation signal of the virtual motor. Meanwhile, a variable-gain terminal SMC is designed to realise the high-speed and high-precision tracking of each filling motor speed to the given signal.

6. Simulation

The simulation of the multimotor system composed of three motors in this section is conducted using MATLAB/Simulink to verify the proposed technical solution on the basis of theoretical studies. The comparative experimental simulation is added in this section to reflect the advantages

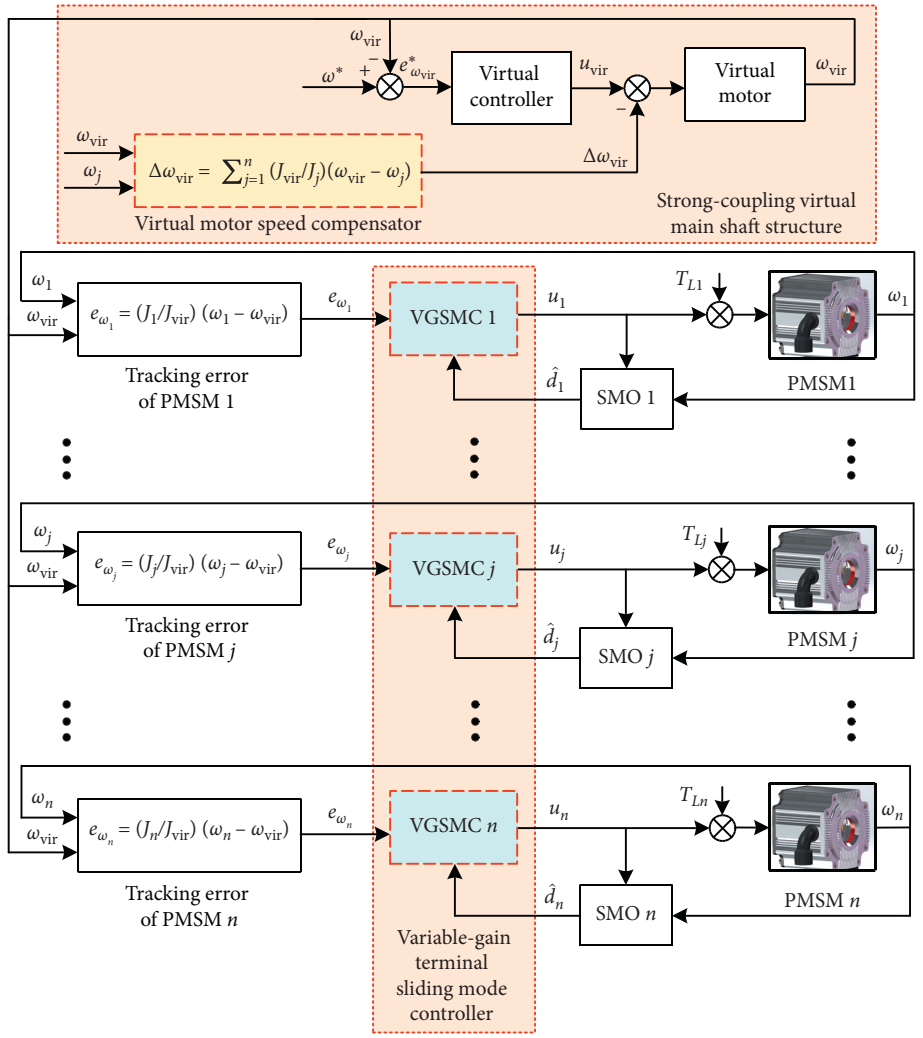

Figure 2: The control block diagram of the improved virtual main shaft structure.

of the improved synchronization topology and the optimised fixed-time controller. The terminal SMC proposed in [43] is used as the reference and modified according to the PMSM model in this study, but the control concept is consistent with the design idea of quotations. The given curve for multimotor system simulation is as follows:

$$\omega^* = \begin{cases} 500t, & 0 \le t < 0.6, \\ 300, & 0.6 \le t < 1.4, \\ -500t + 1000, & 1.4 \le t < 2. \end{cases} \quad (52)$$

Some typical motor parameters are shown in Table 1.

The simulation time in the entire experiment is 2 s. The experimental simulation of the improved virtual main-axis multimotor synchronous control structure is carried out for the optimised variable-gain terminal SMC based on fixed-time convergence and the traditional terminal SMC. The tracking error of each motor is compared with the simulation result of the synchronisation error under the enabling conditions of two controllers. Parameters of the observer are set to $k_1 = 4000$ and $k_2 = 10$. Virtual moment of inertia in the virtual motor is set to $J_{vir} = 0.0001$. The gain of controller

Table 1: Some typical motor parameters.

Parameter	PMSM 1	PMSM 2	PMSM 3
R_Ω (N · m · s)	4.831×10^{-5}	4.846×10^{-5}	4.827×10^{-5}
ψ_f (Wb)	0.175	0.173	0.178
n_p	2	2	2
J (kg · m^2)	8.5×10^{-4}	8.47×10^{-4}	8.51×10^{-4}

in the virtual controller is set to $k_3 = 200$ and $c = 50$. Coefficients of the sliding mode surface in the trial design of the variable-gain terminal SMC are set to $\alpha_1 = \beta_1 = 2.1$, $q_1 = 0.833$, and $g_1 = 2$. Coefficients of the controller are set to $\alpha_2 = \beta_2 = 2.1$, $q_2 = 0.833$, and $g_2 = 2$. The consistency between coefficients of the controller in the designed comparative experiment simulation in [43] and parameters of the observer ensures the validity and preciseness of the comparative experiment. The parameter perturbation value and motor torque variation of motors 1, 2, and 3 are $\Delta a_1 = \Delta b_1 = \Delta T_{L1} = \sin \pi t$, $\Delta a_2 = \Delta b_2 = \Delta T_{L2} = \sin 0.5\, \pi t$, and $\Delta a_3 = \Delta b_3 = \Delta T_{L3} = -\sin \pi t$, respectively. The following will show the simulation results of this experiment in turn.

As shown in Figure 3, motors of the filling multimotor system can successfully track the given value. The designed

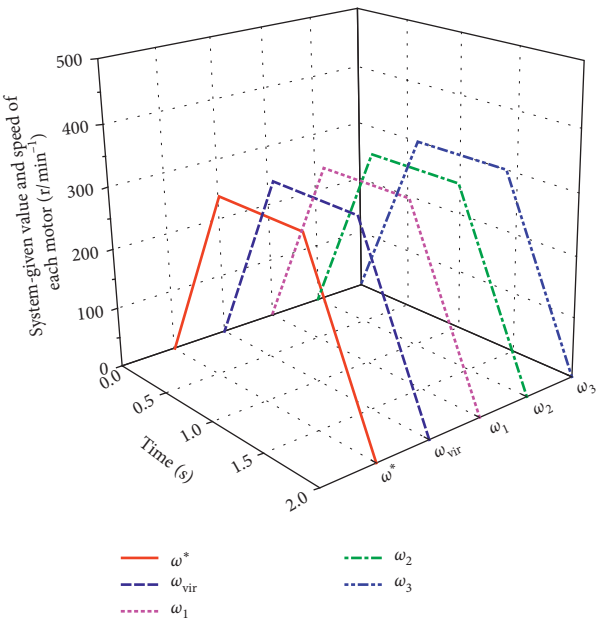

Figure 3: Schematic diagram of speed simulation results of multimotor system.

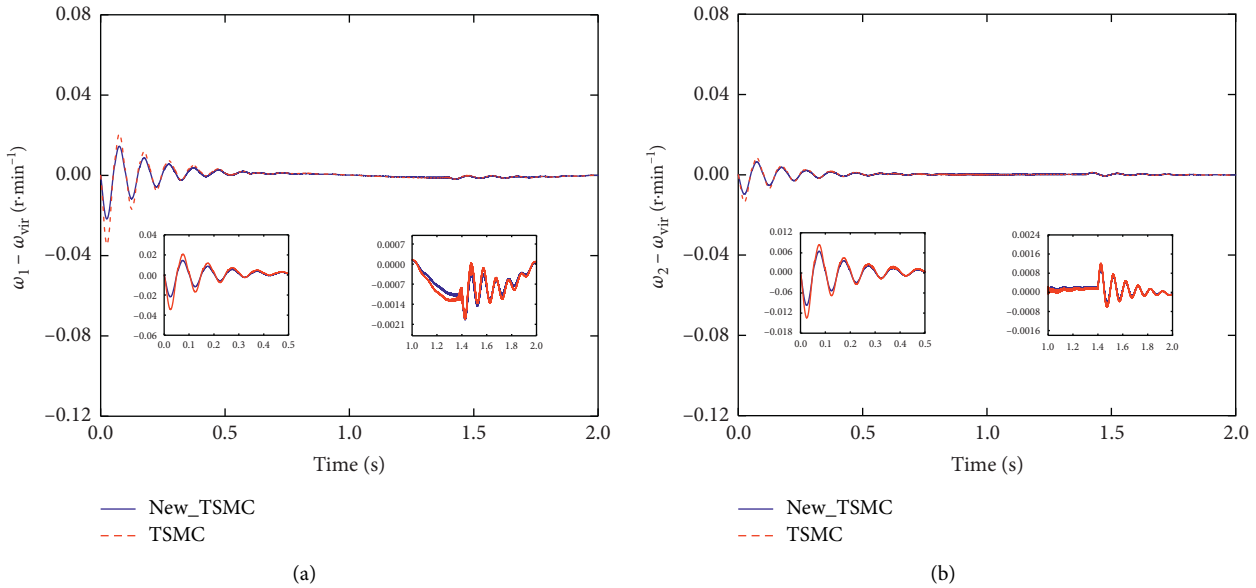

Figure 4: Continued.

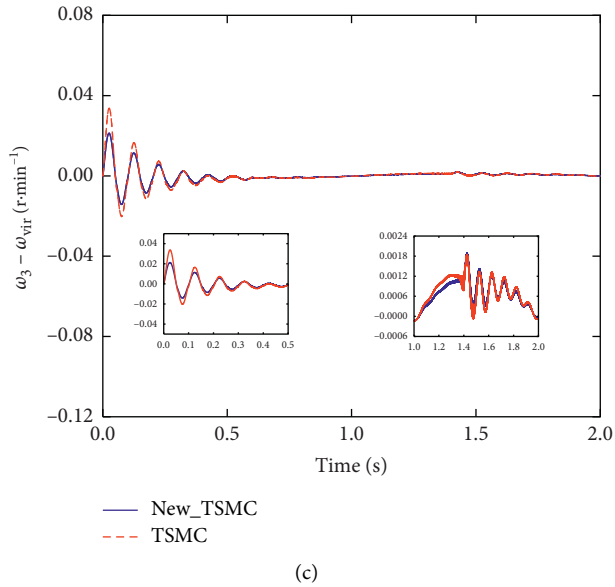

(c)

Figure 4: Simulation comparison of tracking error between (a) motor 1 and virtual motor, (b) motor 2 and virtual motor, and (c) motor 3 and virtual motor.

three-stage given signal includes the following processes: (1) starting and accelerating, (2) running at a uniform velocity, and (3) slowing down to stop. The experimental results showed that virtual and slave motors can rapidly track the given value in the three stages and run stably without evident overshooting. The actual simulation effect of the virtual motor can verify that the selection of the virtual motor's moment of inertia and the design of the virtual controller are reasonable.

Simulation comparison charts in Figures 4(a)–4(c) that present the tracking error of the velocity of motors 1, 2, and 3, respectively, are further representations of the simulation results in Figure 3. New_TSMC and TSMC represent the simulation results of the tracking error between each slave motor and virtual motor under the enabling conditions of the improved variable-gain terminal SMC and controller in [43], respectively. The tracking error of motors 1, 2, and 3 refers to the error between the actual velocity of each motor and the velocity of the virtual motor. The analysis of the simulation results showed that the tracking performance of the improved variable-gain terminal SMC is significantly improved compared with that of the traditional terminal SMC. Both the amplitude of overshooting and the convergence time of all slave motors are reduced by approximately one-third, especially in the initial stage of the simulation.

Figure 5(a) represents the synchronization error between motor 1 and motor 2. Figure 5(b) represents the synchronization error between motor 1 and motor 3. Figure 5(c) represents the synchronization error between motor 2 and motor 3. New_TSMC and TSMC, respectively, represent the simulation results of the synchronisation error between adjacent motors under the enabling condition of the variable-gain terminal SMC and the controller enable condition proposed in [43]. The simulation results showed that the synchronisation performance of the improved controller significantly enhances compared with that of the traditional terminal SMC. Convergence amplitudes of all slave motors are reduced significantly, especially in the initial stage of the simulation.

Figure 6 shows that the tracking error between the real-time speed of the virtual motor and the given value is constantly controlled in a small range and vibrates in a small amplitude of 0.4–1.4 s during start-up, respectively. This phenomenon is mainly caused by the high change rate of the given value signal that causes fluctuation in the velocity of the virtual motor whilst the tracking error of the virtual motor can gradually converge within 0 to 0.001 s. Hence, the convergence is fast and the parameter selection for the virtual motor and the virtual controller is reasonable.

As shown in Figure 7, the velocity compensation signal constantly maintained in a small range is conducive to the design of the gain coefficient of the virtual SMC. This signal is mainly affected by the velocity of all slave motors. Therefore, the velocity compensator signal can only generate a small amplitude of vibration after selecting a small moment of inertia of the virtual motor. The velocity compensation signal gradually converges to zero when the velocity of each motor follows the given value. The result can be used to verify the effectiveness of the design of the velocity compensation signal.

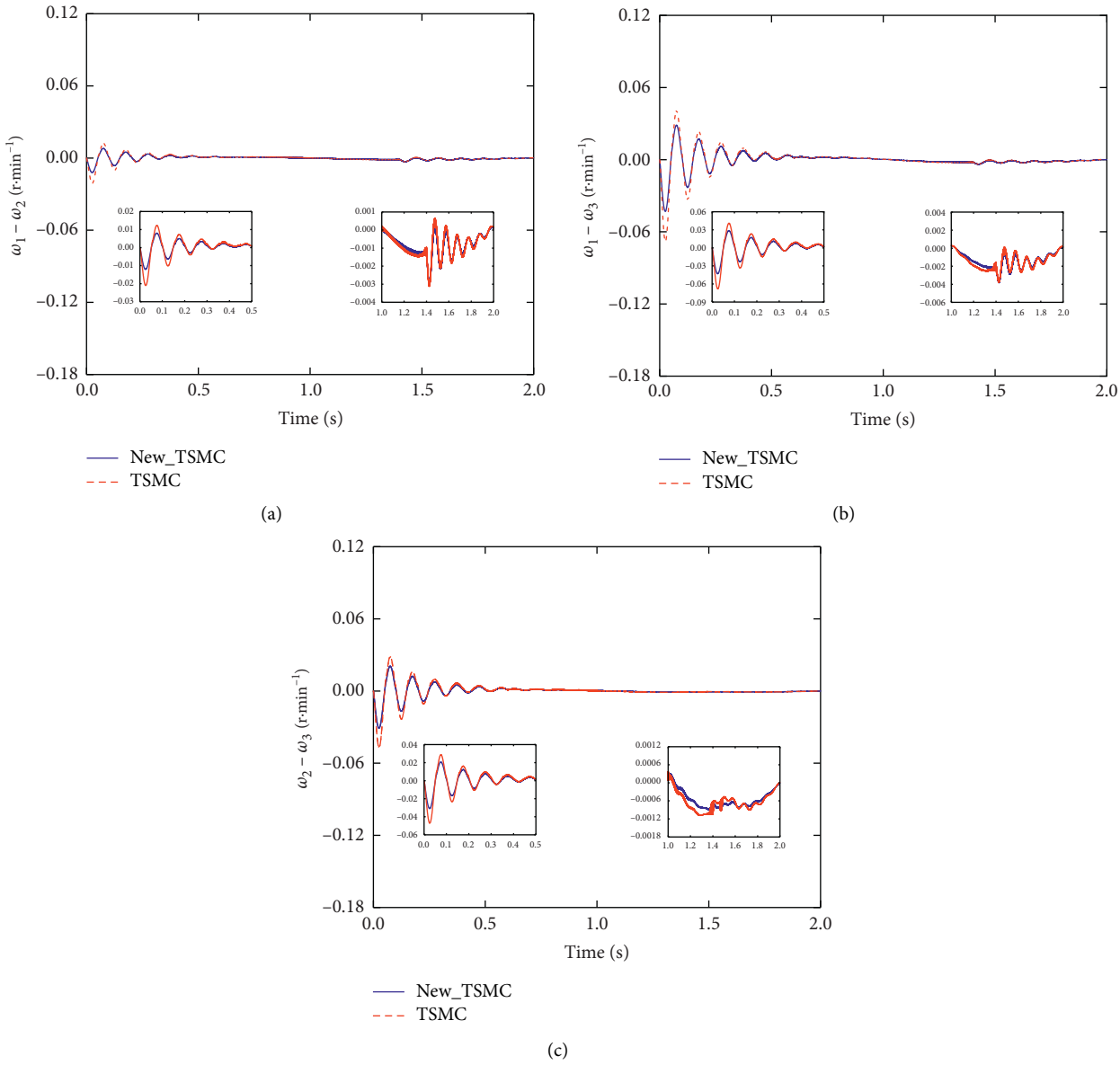

Figure 5: Comparison of simulation diagram of synchronization errors between (a) motors 1 and 2, (b) motors 1 and 3, and (c) motors 2 and 3.

Figures 8(a)–8(c) show the simulation results of disturbances and observed values of motors 1, 2, and 3, respectively. The effect of the estimation of the sliding mode observer of each motor that tracks the actual disturbance is better for different unknown composite disturbances of the three slave motors. The observed value of each motor will evidently jitter in the initial stage of the simulation but can be controlled to follow the actual value of the disturbance within 0.2 s, which exerts a minimal impact on the entire system. This result is consistent with the expectation of the simulation experiment.

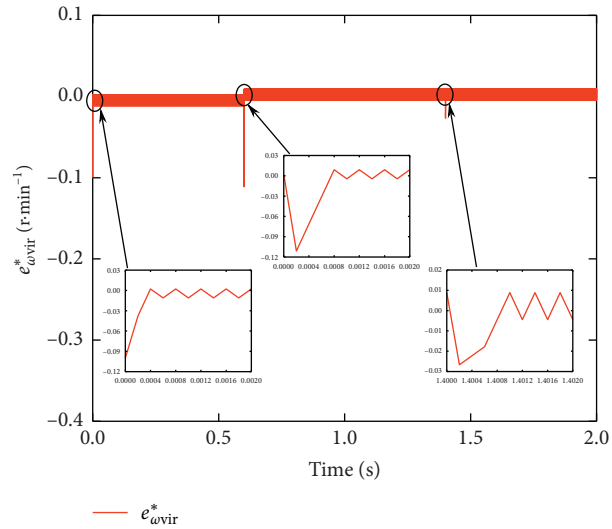

Figure 6: Simulation results of virtual motor speed tracking error.

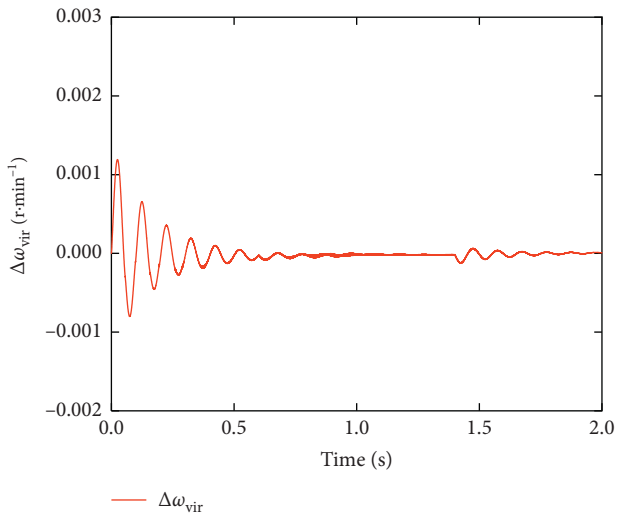

Figure 7: Speed compensator signal simulation results.

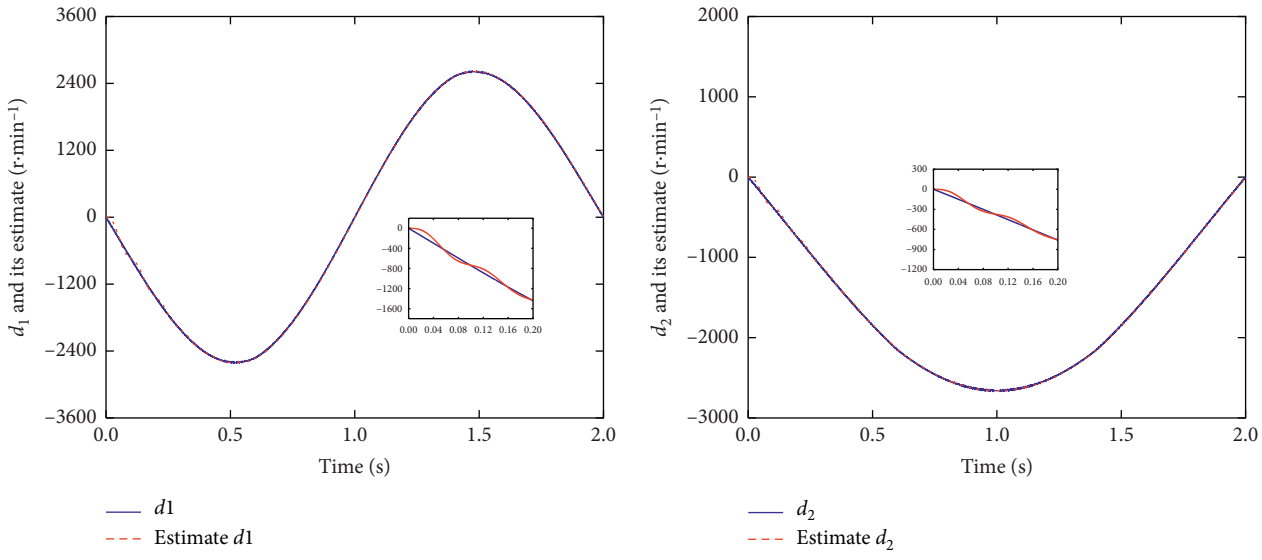

(a) (b)

Figure 8: Continued.

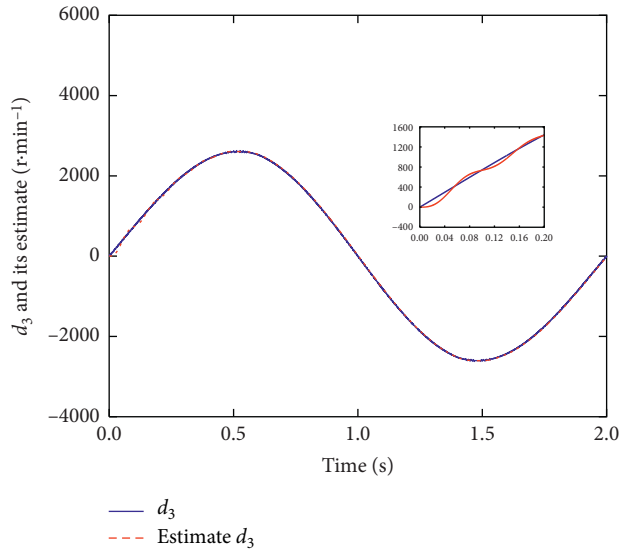

(c)

Figure 8: The disturbance of (a) motor 1, (b) motor 2, and (c) motor 3 and the simulation results of their observations.

7. Conclusions

A novel synchronous control method for the filling multimotor system is put forward in this study. On the one hand, the velocity compensator added to the virtual motor to establish the coupling relationship between virtual and slave motors in the output velocity improves the correlation between systems on the basis of the existing virtual main-axis control structure. On the other hand, the variable-gain terminal sliding mode controller is designed on the basis of the tracking error between each slave motor and the virtual motor to ensure that the multimotor system can be stable within a fixed time. The proposed method can effectively weaken the adverse effects of the system parameter perturbation and motor load variation and improve the convergence robustness performance of the system. Notably, the convergence of each slave motor in the initial stage of the start-up phase significantly improves. The simulation results verify that the method has a relatively prominent effect on the high-performance cooperative control of filling multimotor system.

Data Availability

The model data used to support the findings of this study are available from the corresponding author upon request.

Conflicts of Interest

The authors declare that there are no conflicts of interest regarding the publication of this paper.

Acknowledgments

The study was supported by the National Key R&D Program of China (no. 2018YFD0400705).

References

[1] V. Jerković Štil, T. Varga, T. Benšić, and M. Barukčić, "A survey of fuzzy algorithms used in multimotor systems control," *Electronics*, vol. 9, no. 11, p. 1788, 2020.

[2] Z. Gao, S. K. Nguang, and D. Kong, "Advances in modelling, monitoring, and control for complex industrial systems," *Complexity*, vol. 2019, Article ID 2975083, 3 pages, 2019.

[3] H. R. Karimi, M. Zapateiro, and N. Luo, "Adaptive synchronization of master-slave systems with mixed neutral and discrete time-delays and nonlinear perturbations," *Asian Journal of Control*, vol. 14, no. 1, pp. 251–257, 2012.

[4] Y.-J. Liu, L. Liang, T.-T. Chu, and M.-Y. Wu, "N-PD cross-coupling synchronization control based on adjacent coupling error analysis," *Journal of Central South University*, vol. 25, no. 5, pp. 1154–1164, 2018.

[5] M. Wang, X. Ren, and Q. Chen, "Robust tracking and distributed synchronization control of a multi-motor servo-mechanism with H-infinity performance," *ISA Transactions*, vol. 72, pp. 147–160, 2018.

[6] R. Savelsberg, J. Andert, S. Klein, and S. Pischinger, "Virtual shaft: robust coupling by bidirectional and distributed prediction of coupling values," *Proceedings of the Institution of Mechanical Engineers, Part D: Journal of Automobile Engineering*, vol. 234, no. 10-11, pp. 2419–2428, 2020.

[7] S. Yao, G. Gao, Z. Gao, and S. Li, "Active disturbance rejection synchronization control for parallel electro-coating conveyor," *ISA Transactions*, vol. 101, pp. 327–334, 2020.

[8] J. Xu, H. Lu, and X. Liu, "Synchronization control strategy in multi-layer and multi-axis systems based on the combine cross coupling error," *Advances in Mechanical Engineering*, vol. 9, no. 6, 2017.

[9] Z. Huang, Y. Li, G. Song, X. Zhang, and Z. Zhang, "Speed and phase adjacent cross-coupling synchronous control of multi-exciters in vibration system considering material influence," *IEEE Access*, vol. 7, pp. 63204–63216, 2019.

[10] C. Sun, G. Gong, H. Yang, and F. Wang, "Fuzzy sliding mode control for synchronization of multiple induction motors drive," *Transactions of the Institute of Measurement and Control*, vol. 41, no. 11, pp. 3223–3234, 2019.

[11] L. Tao, Q. Chen, Y. Nan, F. Dong, Y. Jin, and Y. Zhou, "Speed tracking and synchronization of a multimotor system based on fuzzy ADRC and enhanced adjacent coupling scheme," *Complexity*, vol. 2018, Article ID 5632939, 16 pages, 2018.

[12] T. Shi, H. Liu, Q. Geng, and C. Xia, "Improved relative coupling control structure for multi-motor speed synchronous driving system," *IET Electric Power Applications*, vol. 10, no. 6, pp. 451–457, 2016.

[13] C. Zhang, M. Xiao, and J. He, "Multimotor improved relative coupling cooperative control based on sliding mode controller," *Mathematical Problems in Engineering*, vol. 2020, Article ID 5638462, 10 pages, 2020.

[14] C. Xu, Y. Zhao, B. Qin, and H. Zhang, "Adaptive synchronization of coupled harmonic oscillators under switching topology," *Journal of the Franklin Institute*, vol. 356, no. 2, pp. 1067–1087, 2018.

[15] C. Zhang, J. He, L. Jia, C. Xu, and Y. Xiao, "Virtual line-shafting control for permanent magnet synchronous motor systems using sliding-mode observer," *IET Control Theory & Applications*, vol. 9, no. 3, pp. 456–464, 2015.

[16] S. Lin, Y. Cai, B. Yang, and W. Zhang, "Electrical line-shafting control for motor speed synchronisation using sliding mode controller and disturbance observer," *IET Control Theory & Applications*, vol. 11, no. 2, pp. 205–212, 2017.

[17] J. He, X. Chen, S. Mao, C. Zhang, and J. Liu, "Virtual line shafting-based total-amount coordinated control of multi-motor traction power," *Journal of Advanced Transportation*, vol. 2020, Article ID 4735397, 9 pages, 2020.

[18] C. Xu, H. Xu, H. Su, and C. Liu, "Disturbance-observer based consensus of linear multi-agent systems with exogenous disturbance under intermittent communication," *Neurocomputing*, vol. 404, pp. 26–33, 2020.

[19] X. Wang and H. Su, "Completely model-free RL-based consensus of continuous-time multi-agent systems," *Applied Mathematics and Computation*, vol. 382, 2020.

[20] S. Hou, Y. Chu, and J. Fei, "Modified fuzzy neural network control using sliding mode technique for power quality improvement system with experimental verification," *IET Control Theory & Applications*, vol. 14, no. 19, pp. 3029–3037, 2020.

[21] J. He, L. Mi, S. Mao, C. Zhang, and H. Chu, "Fault-tolerant control of a nonlinear system actuator fault based on sliding mode control," *Journal of Control Science and Engineering*, vol. 2017, Article ID 8595960, 13 pages, 2017.

[22] C. Xu, B. Li, and L. Yang, "Semi-global containment of discrete-time high-order multi-agent systems with input saturation via intermittent control," *IET Control Theory & Applications*, vol. 14, no. 16, pp. 2303–2309, 2020.

[23] X. Wang, G.-P. Jiang, H. Su, and Z. Zeng, "Consensus-based distributed reduced-order observer design for LTI systems," *IEEE Transactions on Cybernetics*, pp. 1–11, 2020.

[24] X. Wang, X. Wang, H. Su, and L. James, "Coordination control for uncertain networked systems using interval observers," *IEEE Transactions on Cybernetics*, vol. 50, no. 9, pp. 4008–4019, 2019.

[25] Y. Liu and H. Su, "Containment control of second-order multi-agent systems via intermittent sampled position data communication," *Applied Mathematics and Computation*, vol. 362, 2019.

[26] Y. Liu and H. Su, "Some necessary and sufficient conditions for containment of second-order multi-agent systems with sampled position data," *Neurocomputing*, vol. 378, pp. 228–237, 2020.

[27] Y. Zheng, Y. Song, D. J. Hill, and Y. Zhang, "Multiagent system based microgrid energy management via asynchronous consensus ADMM," *IEEE Transactions on Energy Conversion*, vol. 33, no. 2, pp. 886–888, 2018.

[28] M.-C. Fan and M. Wang, "Second-order consensus for a class of uncertain multi-agent systems subject to input saturation," *Transactions of the Institute of Measurement and Control*, vol. 41, no. 7, pp. 1957–1964, 2019.

[29] Y. Zhai, Z. Liu, Z. Guan, and Z. Gao, "Resilient delayed impulsive control for consensus of multiagent networks subject to malicious agents," *IEEE Transactions on Cybernetics*, pp. 1–10, 2020.

[30] B. Liu, H. Su, F. Jiang, Y. Gao, L. Liu, and J. Qian, "Group controllability of continuous-time multi-agent systems," *IET Control Theory & Applications*, vol. 12, no. 11, pp. 1665–1671, 2018.

[31] G. Shen, Y. Xia, J. Zhang, and B. Cui, "Adaptive fixed-time trajectory tracking control for mars entry vehicle," *Nonlinear Dynamics*, vol. 102, no. 4, pp. 2687–2698, 2020.

[32] X. Shao, B. Tian, and W. Yang, "Fixed-time trajectory following for quadrotors via output feedback," *ISA Transactions*, vol. 110, pp. 213–224, 2021.

[33] J. Sun, J. Wang, P. Yang, and S. Guo, "Model-free prescribed performance fixed-time control for wearable exoskeletons," *Applied Mathematical Modelling*, vol. 90, pp. 61–77, 2021.

[34] Y. Zheng, Y. Song, and D. J. Hill, "A general coordinated voltage regulation method in distribution networks with soft open points," *International Journal of Electrical Power and Energy Systems*, vol. 116, 2020.

[35] R. Rahimilarki, Z. Gao, A. Zhang, and R. Binns, "Robust neural network fault estimation approach for nonlinear dynamic systems with applications to wind turbine systems," *IEEE Transactions on Industrial Informatics*, vol. 15, no. 12, pp. 6302–6312, 2019.

[36] C. Zhang, Q. Zhang, J. He, J. Liu, X. Yang, and S. Mao, "Consistent total traction torque-oriented coordinated control of multimotors with input saturation for heavy-haul locomotives," *Journal of Advanced Transportation*, vol. 2020, Article ID 1390764, 11 pages, 2020.

[37] J. He, C. Zhang, S. Mao, H. Wu, and K. Zhao, "Demagnetization fault detection in permanent magnet synchronous motors based on sliding observer," *Journal of Nonlinear Science Application*, vol. 9, no. 5, pp. 2039–2048, 2016.

[38] B. Jiang, Q. Hu, and M. I. Friswell, "Fixed-time attitude control for rigid spacecraft with actuator saturation and faults," *IEEE Transactions on Control Systems Technology*, vol. 24, no. 5, pp. 1892–1898, 2016.

[39] A. Polyakov, "Nonlinear feedback design for fixed-time stabilization of linear control systems," *IEEE Transactions on Automatic Control*, vol. 57, no. 8, pp. 2106–2110, 2012.

[40] Z. Zhu, Y. Xia, and M. Fu, "Attitude stabilization of rigid spacecraft with finite-time convergence," *International Journal of Robust and Nonlinear Control*, vol. 21, no. 6, pp. 686–702, 2011.

[41] K. Lu and Y. Xia, "Adaptive attitude tracking control for rigid spacecraft with finite-time convergence," *Automatica*, vol. 49, no. 12, pp. 3591–3599, 2013.

[42] L. Liangyong Wang, T. Lianfei Zhai, and L. Zhai, "Neural-network-based terminal sliding-mode control of robotic manipulators including actuator dynamics," *IEEE Transactions on Industrial Electronics*, vol. 56, no. 9, pp. 3296–3304, 2009.

[43] B. Jiang, Q. Hu, and M. I. Friswell, "Fixed-time rendezvous control of spacecraft with a tumbling target under loss of actuator effectiveness," *IEEE Transactions on Aerospace and Electronic Systems*, vol. 52, no. 4, pp. 1576–1586, 2016.